

Loss of Motor Cortical Inputs to the Red Nucleus after CNS Disorders in Nonhuman Primates

 Simon Borgognon^{1,2,3} and Eric M. Rouiller²

¹Center for the Neural Basis of Cognition, Department of Bioengineering, University of Pittsburgh, Pittsburgh, Pennsylvania 15261, ²Department of Neurosciences and Movement Sciences, Section of Medicine, Faculty of Science and Medicine, University of Fribourg, CH-1700 Fribourg, Switzerland, and

³Center for Neuroprosthetics and Brain Mind Institute, École Polytechnique Fédérale de Lausanne, CH-1015 Lausanne, Switzerland

The premotor (PM) and primary motor (M1) cortical areas broadcast voluntary motor commands through multiple neuronal pathways, including the corticorubral projection that reaches the red nucleus (RN). However, the respective contribution of M1 and PM to corticorubral projections as well as changes induced by motor disorders or injuries are not known in nonhuman primates. Here, we quantified the density and topography of axonal endings of the corticorubral pathway in RN in intact monkeys, as well as in monkeys subjected to either cervical spinal cord injury (SCI), Parkinson's disease (PD)-like symptoms or primary motor cortex injury (MCI). Twenty adult macaque monkeys of either sex were injected with the biotinylated dextran amine anterograde tracer either in PM or in M1. We developed a semiautomated algorithm to reliably detect and count axonal boutons within the magnocellular and parvocellular (pRN) subdivisions of RN. In intact monkeys, PM and M1 preferentially target the medial part of the ipsilateral pRN, reflecting its somatotopic organization. Projection of PM to the ipsilateral pRN is denser than that of M1, matching previous observations for the corticotectal, corticoreticular, and corticosubthalamic projections (Fregosi et al., 2018, 2019; Borgognon et al., 2020). In all three types of motor disorders, there was a uniform and strong decrease (near loss) of the corticorubral projections from PM and M1. The RN may contribute to functional recovery after SCI, PD, and MCI, by reducing direct cortical influence. This reduction possibly privileges direct access to the final output motor system, via emphasis on the direct corticospinal projection.

Key words: motor disorders; plasticity; premotor cortex; primary motor cortex; primate; red nucleus

Significance Statement

We measured the corticorubral projection density arising from the PM or the M1 cortices in adult macaques. The premotor cortex sent denser corticorubral projections than the primary motor cortex, as previously observed for the corticotectal, corticoreticular, and corticosubthalamic projections. The premotor cortex may thus exert more influence than primary motor cortex onto subcortical structures. We next asked whether the corticorubral motor projections undergo lesion-dependent plasticity after either cervical spinal cord injury, Parkinson's disease-like symptoms, or primary motor cortex lesion. In all three types of pathology, there was a strong decrease of the corticorubral motor projection density, suggesting that the red nucleus may contribute to functional recovery after such motor system disorders based on a reduced direct cortical influence.

Received Oct. 17, 2022; revised Dec. 14, 2022; accepted Jan. 13, 2023.

Author contributions: S.B. and E.M.R. designed research; S.B. and E.M.R. performed research; S.B. analyzed data; S.B. and E.M.R. wrote the paper.

This work was supported by Swiss National Science Foundation Grants 110005, 132465, 144990, 149643, Sinergia CRSI3_160696, Sinergia Prometheus CRSI33_125408 (E.M.R.), and 210986 (S.B.) and the Swiss Primate Competence Center for Research. We thank Prof. Jocelyne Bloch, Prof. Patrick Freund, Dr. Jean-François Brunet, Dr. Simon Badoud, and Dr. Eric Schmidlin for surgical assistance; Prof. Martin Schwab, Prof. Jocelyne Bloch, Prof. Patrick Freund, Dr. Anis Mir, Dr. Thierry Wannier, Dr. Eric Schmidlin, Dr. Marie-Laure Beaud, Dr. Alexander Wyss, Dr. Shahid Bashir, Dr. Adja Hamadjida, Dr. Aderraouf Belhaj-Saïf, Dr. Mélanie Kaeser, Dr. Julie Savidan, Dr. Anne-Dominique Gindrat, Dr. Yu Liu, Dr. Michela Fregosi, Dr. Simon Badoud, Alessandro Contestabile, and Jérôme Cottet for contributions to experimental sessions and elaborations of experimental protocols; Laurent Bossy, Jacques Maillard, Bernard Bapst, Bernard Morandi and Joseph Corpataux for animal care assistance; Christine Roulin, Véronique Moret, and Christiane Marti for tissue processing; Felix Meyenhofer for technical microscopical assistance; and Dr. Erinn M. Grigsby for proofreading.

The authors declare no competing financial interests.

Correspondence should be addressed to Simon Borgognon at simon.borgo@pitt.edu.

<https://doi.org/10.1523/JNEUROSCI.1942-22.2023>

Copyright © 2023 the authors

Introduction

The multiple motor cortical areas in primates broadcast commands through parallel neuronal pathways to generate and coordinate voluntary movements (Luppino and Rizzolatti, 2000; Dum and Strick, 2002; Rouiller, 2012). These routes reach multiple regions of the CNS including subcortical relays, the brainstem, and the spinal cord. These projections are specifically organized depending on their origin and their targets (Lemon, 2008). For instance, in intact macaques, the premotor cortex (PM) sends denser projections to the subthalamic nucleus (Borgognon et al., 2020), the superior colliculus (Fregosi and Rouiller, 2017), and the reticular formation (Fregosi et al., 2017) than the primary motor cortex (M1). After motor disorders, these projections undergo unique regional plasticity that depends on the

lesion type, the severity of the symptoms, and the application of a tentative treatment. First, the density of M1-corticobulbar projection increases after spinal cord injury (SCI), regardless of the presence of anti-Nogo-A antibody treatment, whereas it reduces in the case of Parkinson's disease (PD)-like symptoms treated with autologous cellular therapy (Fregosi et al., 2018). The corticobulbar projection arising from PM reduces after either M1 injury or PD-like symptoms treated with cellular therapy (Fregosi et al., 2018). Second, following primary motor cortex injury (MCI), the corticotectal projection density from PM to the superior colliculus reduces when treated with anti-Nogo-A antibody but does not change in absence of treatment (Fregosi et al., 2019). In cases of PD-like symptoms treated with autologous cellular therapy, there is no consistent impact on the corticotectal projections arising from PM or M1 (Fregosi et al., 2019). Third, the projections from M1 or PM to the subthalamic nucleus reorganize in a severity-of-lesion manner in PD monkeys treated with autologous cellular therapy, reduction of density after low symptoms and increase of density after severe symptoms (Borgognon et al., 2020). Region-specific plasticity represents therefore a key neural mechanism that needs to be further investigated. Indeed, new findings can illuminate fundamental principles and may lead to the development of new targeted therapeutic avenues.

Among the subcortical structures receiving direct motor cortical inputs, the red nucleus (RN) constitutes a major player in movement and programming function through the rubrospinal and rubro-olivo-cerebellar systems (for review, see Basile et al., 2021). In primates, evolutionary constraints lead to a complete anatomic segregation of the RN consisting of a magnocellular part (mRN) and a parvocellular part (pRN; ten Donkelaar, 1988; Massion, 1988; Gruber and Gould, 2010) with the latter receiving denser motor cortical projections than mRN (Humphrey et al., 1984).

However, the respective contributions of M1 and PM to the corticorubral projections is not known. Furthermore, the axonal endings topography of these corticorubral projections has not been quantified. Finally, although RN plays a role after PD (Wang et al., 2016; Guan et al., 2017; Philippens et al., 2019) and pyramidal lesion (Yeo and Jang, 2010; Rüber et al., 2012), how the corticorubral projections reorganize following motor disorders has not been established in primates.

What is the topography and density of the corticorubral projections arising from M1 and PM to the RN? What is the impact of a CNS disorder affecting the motor system on these projections? To answer these questions, we injected 20 adult macaques with the biotinylated dextran amine (BDA) anterograde tracer either in PM or in M1 (Extended Data Table 1-1). To quantify the axonal terminal boutons and en passant boutons within the RN, we developed an algorithm that detects BDA-stained axonal boutons in pRN and mRN, separately. We first compared the axonal bouton density in the bilateral pRN or mRN arising from PM or M1 in six healthy monkeys. In the same monkeys, we quantified the topography of axonal boutons along the dorsoventral and mediolateral axes. We next compared the axonal bouton density differences between the healthy group and (1) four M1 or PM injected monkeys after inducing PD-like symptoms, (2) six M1 injected macaques after inducing cervical SCI, and (3) four PM injected macaques subjected to an MCI.

Materials and Methods

Animals and BDA surgical procedures. All surgical experimental procedures, experiments, and animal care were conducted in accordance

with the ethical guidelines (1996) and authorized by the local (Canton of Fribourg) and federal (Switzerland) veterinary authorities (Authorizations FR_44_92_3; FR_156_00; FR_156_02; FR_156_04; FR_156_06; 156_08E; FR_157_03; FR_157_04; FR_157e_04; FR_185_08; 17_09_FR; 2012_01-FR; 2012_01E_FR). The conditions of housing in the animal facility were described earlier in detail (Borgognon et al., 2017; <https://tube.switch.ch/videos/2d5bb2d6>). The materials and methods are similar to those reported in publications related to the corticobulbar (corticoreticular; Fregosi et al., 2017, 2018), corticotectal projections (Fregosi and Rouiller, 2017; Fregosi et al., 2019), and hyperdirect cortico-subthalamic pathway (Borgognon et al., 2020). Briefly, surgeries were performed under sterile conditions in anesthetized adult macaque monkeys of either sex (individual data for each monkey are listed in Extended Data Table 1-1). The protocol consisted of multiple injections of the anterograde tracer BDA (MW, 10,000; Molecular Probe) unilaterally in PM or M1, using a 10 μ l Hamilton microsyringe. BDA concentration was 5% (in distilled water) for monkey M93-80 and 10% for the other monkeys. The extent of the BDA injection site was assessed on consecutive histologic frontal sections, each reconstructed manually using NeuroLucida software (version 11, MBF Bioscience). Three-dimension (3D) reconstruction was performed by stacking on a dorsolateral view the mediolateral extent of BDA intake from the midline. The injection sites in PM involved both dorsal PM (PMd) and ventral PM (PMv) in most monkeys, except in monkeys R12, LL, and RO in which BDA was delivered mostly in PMd. The BDA injection in M1 was limited to the hand area in monkeys M93-80 and CS, as defined by intracortical microstimulation. For the other M1 injections, based on anatomic landmarks (cortical sulci), BDA involved the hand area as well as more proximal territories of the forelimb.

Lesion and treatment procedures. The first lesion group was composed by six macaque monkeys (CS, CP, CG, AC, AG, and AP) that underwent an SCI at C7–C8 level (hemisection). This SCI group (Extended Data Table 1-1) was further subdivided into a control subgroup ($n = 3$; monkeys CS, CP, and CG) and a subgroup subjected to an anti-Nogo-A antibody treatment ($n = 3$; monkeys AC, AG, and AP; Freund et al., 2006, 2007, 2009). The surgical, lesion, and behavioral procedures have been previously reported in (Freund et al., 2006, 2007; Beaud et al., 2008). Briefly, the six monkeys were treated with antibodies (control or anti-Nogo-A) applied intrathecally by infusion over 4 weeks into the subdural space of the lower cervical spinal cord. In both subgroups, the treatment was delivered with an osmotic pump (2 ml; 2ML2, ALZET) located in the back of the animal 3–5 mm rostral to the cervical lesion site and connected to it by a SILASTIC tube. The implantation of the osmotic pump was performed a few minutes after the cervical lesion itself.

The surgical, lesion, and behavioral procedures of the group of four macaque monkeys (LL, MY, LY, and MI) subjected to PD-like symptoms have been previously reported (Badoud et al., 2017; Borgognon et al., 2017, 2019). Briefly, the four monkeys underwent daily 1-methyl-4-phenyl-1,2,3,6-tetrahydropyridine (MPTP; 0.5 mg/kg i.m.; Sigma-Aldrich; duration: \sim 1 month) injections with the purpose to kill dopaminergic neurons in the substantia nigra pars compacta (SNpc). At the end of the lesional protocol the monkeys had received between 6.25 ml/kg and 7.75 mg/kg of MPTP. The protocol consisted of two series of injections for 4d each with a break after the fourth day. All safety protocols were adapted in accordance with the National Institutes of Health. After a stable plateau of incomplete spontaneous functional recovery was reached, the four monkeys were treated with autologous neural cell ecosystems (ANCE) obtained by cell culture of cortical neurons developed *in vitro* from cortical biopsies (Brunet et al., 2002, 2005, 2009; Bloch et al., 2011, 2014; Kaeser et al., 2011; Badoud et al., 2017; Borgognon et al., 2017, 2019). ANCE was then reimplanted in the same monkey. The injection sites (two in the putamen and one in the caudate nucleus on each side) were identified by aid of postlesional T1-weighted MRI scan (OsiriX, version 4.1.2) and confirmed by the Paxinos atlas (Paxinos et al., 2000). Cells were implanted via a Hamilton microsyringe (10 μ l culture medium; 2 μ l/min during 5 min per injection site) using a nanoinjector (Stoelting) fixed to a stereotaxic frame. Each monkey received between 250,000 and 400,000 cells. At the end of the

protocol, two of the PD monkeys were injected unilaterally with BDA in PM (LL, MY) and the other two monkeys in M1 (LY, MI).

Finally, a group (MCI) of four macaques, subjected to an M1-injury (hand area), were injected in PM with BDA unilaterally (Extended Data Table 1-1). Two MCI monkeys (VA and MO) received an anti-Nogo-A antibody treatment, and two MCI monkeys (RO and BI) were untreated (controls). All MCI monkeys were implanted with chronic chambers fixed to the skull for easier access to the hand region of M1. Cortical lesion of M1 hand area was obtained by multiple injections of ibotenic acid (10 $\mu\text{g}/\mu\text{l}$ in PBS) with a 10 μl Hamilton syringe at multiple sites corresponding to digit areas previously identified by intracortical microstimulation, as previously reported (Hamadjida et al., 2012; Wyss et al., 2013). VA and MO were treated with anti-Nogo-A antibodies (3 mg/ml) administered by two osmotic pumps (5 $\mu\text{l}/\text{h}$; model 2ML2, ALZET) implanted under anesthesia in a subcutaneous pouch in the neck region. One pump administered the treatment intrathecally to the cervical spinal cord, whereas the other pump delivered the antibody close to the lesion site in M1 below the dura. The treatment was delivered for a total duration of 4 weeks before surgical removal of the two osmotic pumps. The treatment was delivered immediately after the lesion, thus the surgery for pump implantation followed the injection of ibotenic acid.

Histologic procedures. At the end of the experimental protocols, after completion of behavioral and electrophysiological investigations, BDA injections, and survival time to allow axonal transport of BDA, the monkeys were killed under lethal anesthesia. Surgical procedures for killing were previously reported (Freund et al., 2006, 2007; Beaud et al., 2008; Hamadjida et al., 2012; Wyss et al., 2013; Borgognon et al., 2017). Briefly, the monkeys were subjected to transcardiac perfusion with 400 ml, 0.9% saline, followed by 3 L of 4% paraformaldehyde (0.1 M phosphate buffer, pH 7.6) and finally three series of 2 L each of sucrose solutions (10, 20, and 30%) to fix and cryopreserve the tissue. The brains were cut in the frontal plane in 50- μm -thick sections with a freezing microtome, collected in five to seven series. One series of brain sections was processed to visualize BDA to reconstruct the location of stem axons and axonal boutons, both en passant and *terminaux* (histochemical protocol described in Rouiller et al., 1994). Another series of sections was used to stain for Nissl bodies to visualize the cytoarchitecture of the RN. All monkeys showed a significant BDA uptake as described in our previous publications (Fregosi et al., 2018, 2019; Borgognon et al., 2020) and as shown by the fairly comparable numbers of corticospinal axons in the pyramids in the intact and in the injured monkey groups (Extended Data Table 1-1).

Data collection and analysis. To quantify the synaptic terminal and en passant axonal boutons within the RN, we developed an algorithm that detects BDA-stained boutons. We imaged the histologic sections (Nissl and BDA stained) with the bright field microscope slide scanner Leica DM6 B Navigator, camera DMC5400, and LAS X Navigator software at magnification of 10 \times . We analyzed all the histologic sections within the two Nissl and BDA series covering the RN in the intact monkeys. Because of the low (or inexistent) number of axonal boutons in the injured monkeys (SCI, PD, MCI), we analyzed only sections where we found axonal boutons. If a monkey did not show any axonal boutons, we performed the analysis in four sections only. For all the subsequent analysis we used MATLAB R2019a. First, the images were converted into JPEG format from their original LIF format. Then, we manually coregistered the two corresponding BDA and Nissl-stained sections and defined the pRN and mRN contours on the resulting images. Based on the contours, we extracted the pRN and mRN and converted the images in grayscale. We then converted the grayscale images into binary images by applying a threshold of gray pixel intensity. Different thresholds were tested on few random sections for each monkey. We choose the optimal threshold by visually verifying that the resulting binary image captured actual axonal boutons. Once the threshold was defined, we applied the same threshold for all the sections in each monkey and obtained the binary images. As BDA protocol may result in staining artifacts (e.g., blood vessels and neurons), we applied two filters, (1) a size filter of conglomerated pixels with a lower and upper size limit of 2 and 400 pixels, respectively, and (2) a circularity, C , filter of conglomerated pixels of 0.5 (1 being a perfect circle) based on the following formula:

$$C = \frac{4 * \pi * A}{P^2},$$

where C is the circularity, A is the area of the conglomerated pixels, and P is the perimeter of the conglomerated pixels. These two parameters were kept for all histologic sections in all monkeys. We tested the accuracy and validity of the algorithm by comparing in one intact monkey (CH) the numbers of axonal boutons obtained either with the present algorithm or by manually charting all axonal boutons using the manual exhaustive plotting method in RN as we did previously in studies on the corticoreticular, corticotectal, and corticosubthalamic projections (Fregosi et al., 2018, 2019; Borgognon et al., 2020). We obtained consistent results with the two methods, attested by comparable distributions of axonal boutons along the rostrocaudal axis of RN in monkey CH. The present automated and the previous manual (Fregosi et al., 2018, 2019; Borgognon et al., 2020) counting methods both consist of an exhaustive sampling approach of axonal boutons in a given target nucleus, for which stereology is not pertinent. We then normalized in each monkey the number of axonal boutons in RN with the number of corticospinal axons labeled just above the pyramidal decussation (Extended Data Table 1-1) as described in previous reports (Fregosi et al., 2017, 2018, 2019; Fregosi and Rouiller, 2017; Borgognon et al., 2020). The axonal bouton density of each section was obtained by counting the number of axonal boutons in a 2500 μm^2 area. For each histologic section, we divided pRN and mRN into four quadrants, dorsolateral, dorsomedial, ventrolateral, and ventromedial parts. To compare the density topography across sections, we interpolated (MATLAB function interp1) the density of each quadrant into equal sizes and plotted the average density across sections. The density of each section was measured with the area under the curves (AUC; MATLAB function trapz). Because of the low number of monkeys, we performed a bootstrapping analysis, where the initial population of n analyzed histologic sections, covering the rostrocaudal extent of the pRN or mRN, was resampled with replacement to obtain $k = 100,000$ fictive populations of n sections independently for each monkey. For each bootstrapped population, we summed up the number of BDA-labeled boutons along the rostrocaudal axis to finally obtain the total number of BDA-labeled boutons of the 100,000 bootstrapped populations. As standard in bootstrapping, we calculated the p value by estimating the residuals of the combined distribution testing for the null hypothesis that the Gaussian distribution of the difference had a mean value of 0 as follows:

$$p = \int_{-\infty}^0 N\left(\mu_1 - \mu_2, \frac{\sigma_1^2 + \sigma_2^2}{2}\right) + \int_0^{+\infty} N\left(\mu_2 - \mu_1, \frac{\sigma_1^2 + \sigma_2^2}{2}\right),$$

where N is the Gaussian distribution function, μ_1 and μ_2 are the means of the two conditions with $\mu_1 > \mu_2$ and σ_1 and σ_2 are their respective SDs. Finally, the significance threshold of the p value has been adjusted using the Bonferroni correction for multiple-group comparisons ($\alpha = 0.05$ divided by the number of groups). This bootstrapping methodology has been previously performed in another report (Borgognon et al., 2020). Some analyses did not require a bootstrapping analysis (e.g., the comparison between the number of axonal boutons across intact monkeys). We therefore used the standard Wilcoxon signed-rank test. The performed statistical tests as well as the α thresholds after Bonferroni correction are mentioned in the captions of each plot.

Results

To quantify the corticorubral projections, we used six healthy macaques unilaterally injected with the anterograde tracer BDA in M1 or in PM (Fig. 1a; each individual BDA uptake reconstruction provided in Extended Data Fig. 1-1), in which the cortico-subthalamic (Borgognon et al., 2020), corticotectal (Fregosi and Rouiller, 2017), and corticoreticular (Fregosi et al., 2017) projections were previously quantified. The identities of the six intact

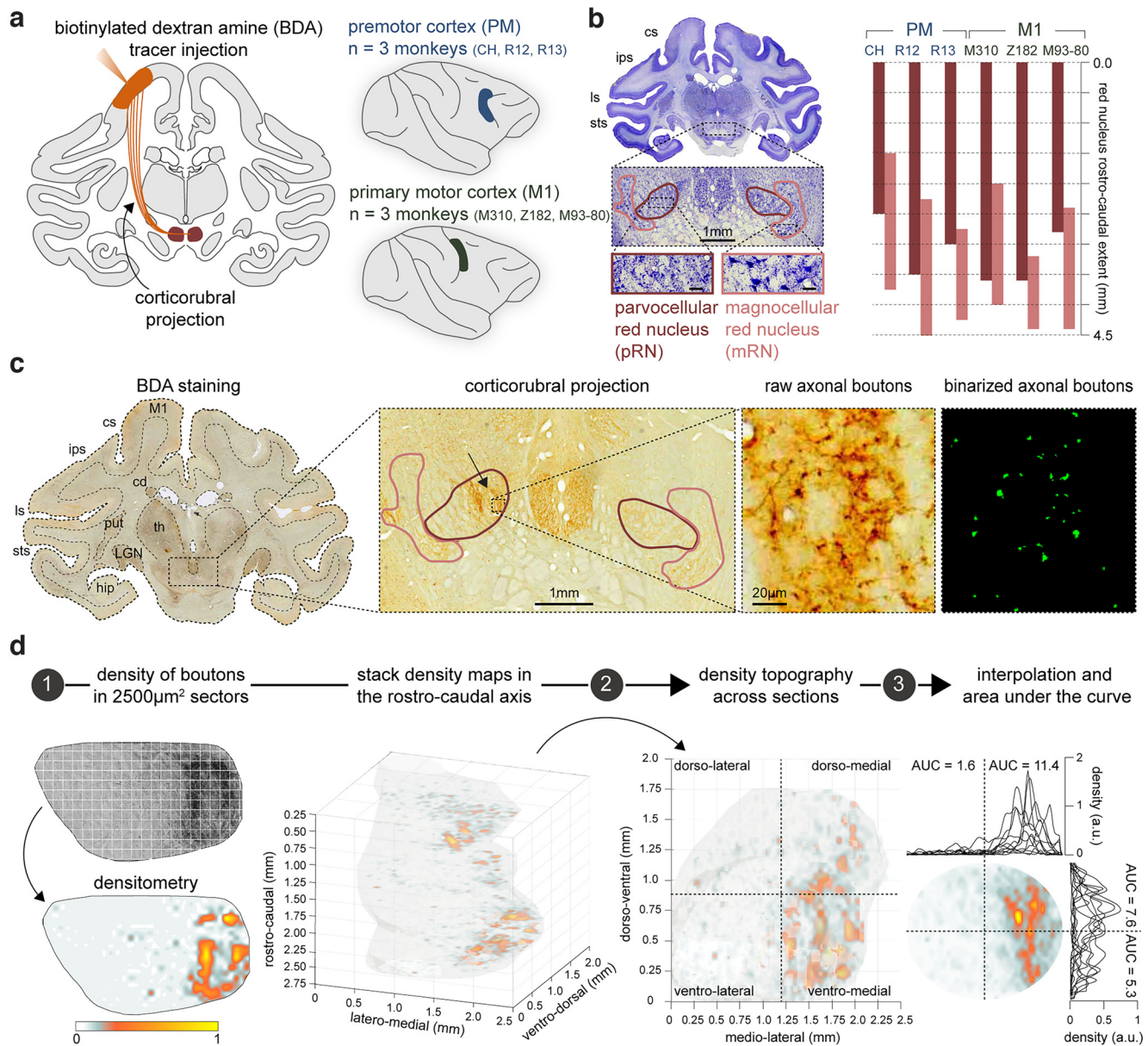


Figure 1. Experimental framework and methodology (illustrated for the six intact monkeys). **a**, Left, Schematic representation of the corticorubral projection in a frontal brain section. Right, we unilaterally injected the anterograde tracer BDA in PM or M1, as schematically represented. Three monkeys (CH, R12, and R13) were injected in the PM, and three other monkeys (M310, Z182, and M93-80) were injected in the M1. Injection site reconstructions for each monkey are shown in Extended Data Figure 1-1. **b**, Left, Representative example of a Nissl-stained histologic section showing the segregation between pRN (dark red) and mRN (light red). Scale bar, 100 μ m. Right, Rostrocaudal extent of the red nucleus for each of the six monkeys. More examples of histologic sections are shown in Extended Data Figure 1-2. **c**, Semiautomated algorithm to detect axonal boutons (Extended Data Figure 1-3; see above, Materials and Methods). Left, Corresponding BDA-stained histologic section of **b**, Middle left, Magnification of the red nucleus showing the corticorubral projection (black arrow). Middle right, Magnification of axonal boutons located in the ipsilateral pRN. Far right, Binarized axonal bouton detection based on the intensity, the circularity, and the size of conglomerated pixels. **d**, Methodology to compute topography of the corticorubral projections. Step 1 (1), we computed the density of boutons for each histologic section. Step 2 (2), we stacked all the sections on the rostrocaudal axis. Step 3 (3), for each histologic section, we divided pRN and mRN into four quadrants—dorsolateral, dorsomedial, ventrolateral, and ventromedial parts. To compare the density topography across sections, we interpolated (see above, Materials and Methods) the density of each quadrant into equal sizes and plotted the average density across sections. The density of each section was measured with the AUC.

monkeys are listed in Extended Data Table 1-1, with a more precise location of the BDA injection sites in PM (PMd, PMv) or in M1 (hand/arm area). In each monkey, we identified the pRN and the mRN based on a series of Nissl-stained histologic sections (Fig. 1*b*, left) and measured the total rostrocaudal extent of each substructure. The total rostrocaudal lengths of the RN across the six intact monkeys were 3.75 mm (CH), 4.5 mm (R12), 4.25 mm (R13), 4.0 mm (M310), 4.4 mm (Z182), and 4.4 mm (M93-80; Fig. 1*b*, right). As expected, the pRN was located more rostrally than the mRN and covered about two third of the

total RN. The mRN occupied the caudal portion of the RN and represented about one-third of the total RN (Fig. 1*b*, right; Extended Data Fig. 1-2). An adjacent series of BDA-stained histologic sections that spanned the RN allowed us to visualize the axonal boutons emitted by the corticorubral axons (Fig. 1*c*; Extended Data Fig. 1-3). We then coregistered BDA-stained sections with their corresponding Nissl-stained sections. On the coregistered images, we manually defined the pRN and mRN contours and extracted the RN (Extended Data Fig. 1-3). We developed an algorithm that detected the intensity, the size, and

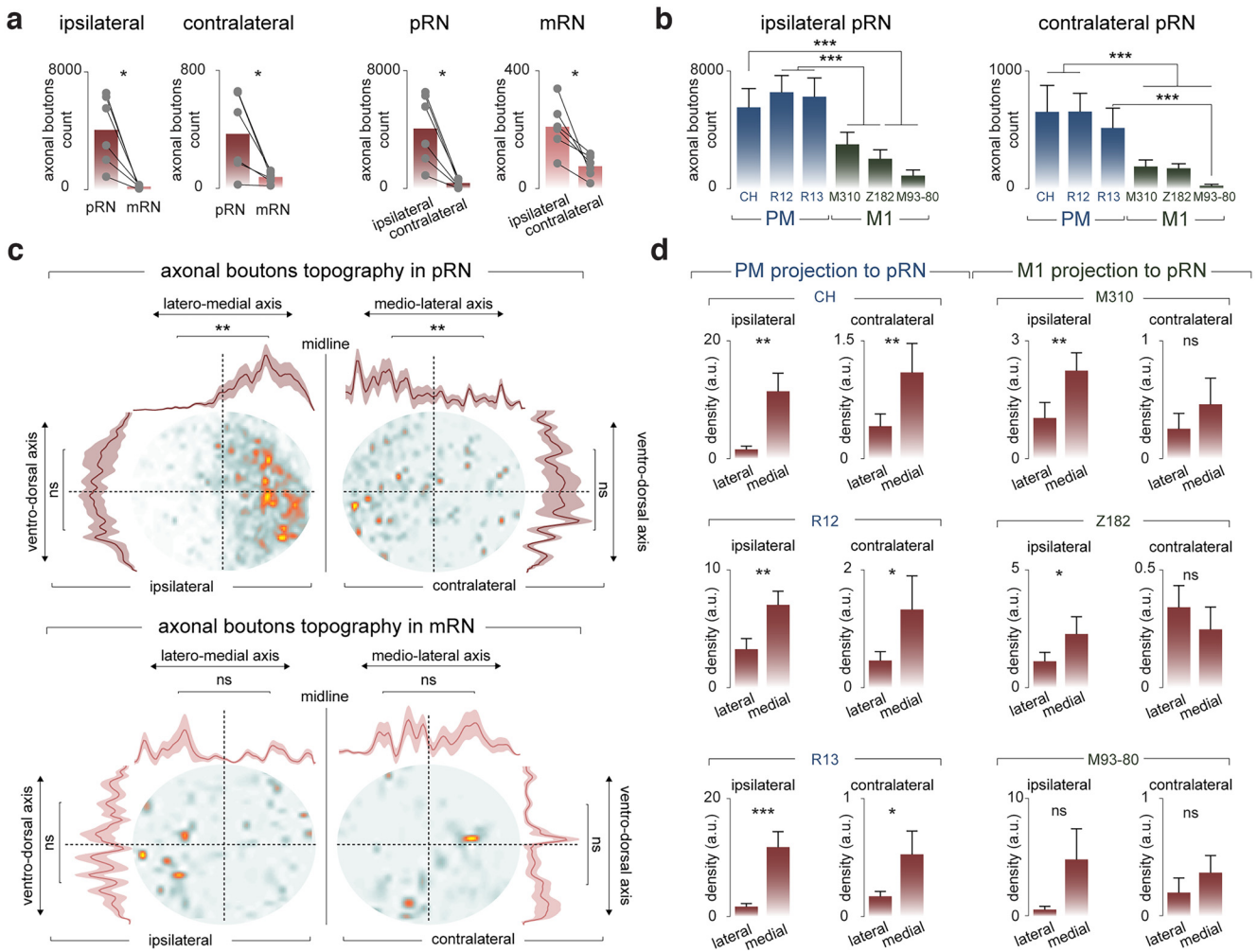


Figure 2. Corticorubral projection density and topography in the six intact monkeys. **a**, Bar plots showing the mean axonal bouton count across monkeys (gray dots). Statistically significant differences are indicated ($*p \leq 0.05$, Wilcoxon signed-rank test). **b**, Bar plots showing the means + SDs of axonal bouton count for each individual monkey across bootstrapped histologic sections (see above, Material and Methods). Statistically significant p values are indicated ($***p < 0.00016$, residual estimation of the combined distributions and Bonferroni correction for multiple-group comparisons). **c**, Axonal bouton topography in one representative monkey (CH). The curves show the mean (solid line) \pm SE (shaded areas) across histologic sections. The density differences between medial versus lateral and dorsal versus ventral are shown ($**p \leq 0.01$, Wilcoxon signed-rank test. ns, Not significant (p values > 0.05)). **d**, Axonal bouton topography in pRN for each individual monkey. Statistically significant differences are indicated ($*p \leq 0.05$, $**p \leq 0.01$, $***p \leq 0.001$; ns, $p > 0.05$; Wilcoxon signed-rank test).

the circularity of conglomerated pixels to quantify the axonal terminal boutons and en passant boutons (see above, Materials and Methods; Fig. 1c; Extended Data Fig. 1-3). The axonal bouton sizes were comparable to the ones found in either the reticular formation, the subthalamic nucleus, the superior colliculus, or the vast majority of boutons in the thalamus but were much smaller than the few giant endings terminating in the thalamus (Rouiller et al., 1998). Finally, we computed the density of axonal boutons in 2500 μm^2 sectors to generate a density map for each section (Fig. 1d, left, step 1). For each histologic section, we divided pRN and mRN into four quadrants—dorsolateral, dorsomedial, ventrolateral and ventromedial (Fig. 1d, middle, step 2). To compare the density topography across sections, we interpolated (see above, Materials and Methods) the density of each quadrant into equal sizes and plotted the average density across sections (Fig. 1d, right, step 3). The density of each section was measured with the AUC (see above, Materials and Methods; Fig. 1d).

Intact monkeys

In all intact monkeys ($n = 6$), the ipsilateral pRN represented the preferred corticorubral target regardless of the

injected motor cortical area (mean across monkeys = 4056 axonal boutons). The second most predominant projection reached the contralateral pRN with an average of 368 axonal boutons across all six intact monkeys. The mRN represented only a small proportion of axonal boutons (means were 210 and 76 axonal boutons for the ipsilateral and contralateral mRN, respectively; Fig. 2a; p value < 0.05 ; Wilcoxon signed-rank test). Detailed analyses for each intact monkey separately are shown in Extended Data Fig. 2-1). Each monkey showed a comparable distribution of axonal boutons along the rostrocaudal axis (Extended Data Fig. 2-1a). We performed the same analysis as shown in Figure 2a but for each monkey separately. All intact monkeys showed statistically significant differences between all the paired comparisons possible except for ipsilateral mRN versus contralateral mRN in R12 and R13, and contralateral pRN versus contralateral mRN in M93-80 (Extended Data Fig. 2-1b; p values < 0.05 , residual estimation of the combined bootstrapped distributions).

Within each injection subgroup (PM or M1), the monkeys yielded comparable numbers of axonal boutons in

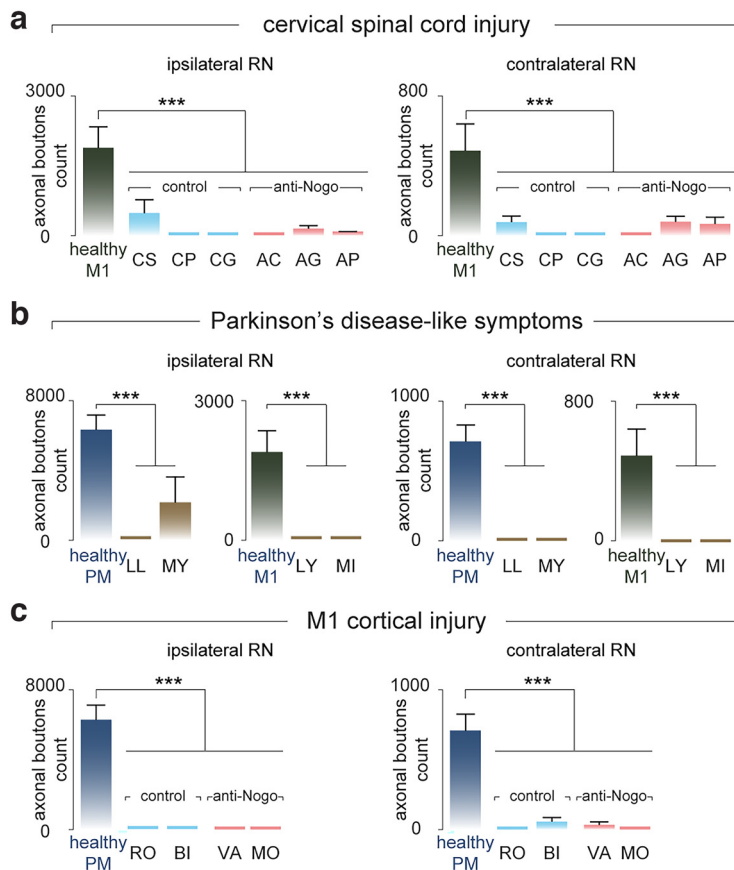


Figure 3. *a–c*, Corticorubral projection plasticity after cervical spinal cord injury, Parkinson's disease-like symptoms and M1 injury. Bar plots showing the means + SDs of axonal bouton count across bootstrapped histologic sections (see above, Materials and Methods). Statistical significance is shown (*** $p < 0.0071$ in *a*, *** $p < 0.016$ in *b*, and *** $p < 0.01$ in *c*; residual estimation of the combined distributions and Bonferroni correction for multiple-group comparisons). As a result of only a few counts of axonal boutons in the injured monkeys, we pooled the count of axonal boutons of pRN and mRN. The lesion extent and the BDA reconstruction uptake are shown in Extended Data Figure 3-1. *a*, Comparison between intact monkeys injected in M1 ($n = 3$; mean value) and individual monkeys subjected to a unilateral cervical spinal cord injury ($n = 6$). The spinal cord injury group was further subdivided into two groups, a control group ($n = 3$; CS, CP, and CG, light blue) that received sham treatment and a group treated with anti-Nogo-A antibody ($n = 3$; AC, AG, and AP, light red; Freund et al., 2006, 2007; Beaud et al., 2008). *b*, Comparison between intact monkeys injected in M1 ($n = 3$, average value) or PM ($n = 3$, average value) and four individual monkeys exhibiting Parkinson's disease-like symptoms and treated with ANCE (Borgognon et al., 2017, 2019). *c*, Comparison between three intact monkeys unilaterally injected in PM (average value) and four individual monkeys after a unilateral M1 cortical injury induced with acid ibotenic. The BDA injection was performed in PM homolateral to the injured M1. The M1 cortical injury group was further subdivided into two subgroups, an untreated control subgroup ($n = 2$; RO and BI, light blue) and a subgroup treated with anti-Nogo-A antibody ($n = 2$, VA and MO, light red; Hamadjida et al., 2012; Wyss et al., 2013).

pRN (statistically nonsignificant; p values > 0.0083 ; residual estimation of the combined bootstrapped distributions and Bonferroni correction for multiple-group comparisons; see above, Materials and Methods). However, the number of axonal boutons originating from PM was higher than those from M1 (p values < 0.0083 , residual estimation of the combined bootstrapped distributions and Bonferroni correction for multiple-group comparisons) in all two by two intermonkey comparisons, except CH compared with M310 (Fig. 2*b*; p value > 0.0083 , residual estimation of the combined bootstrapped distributions and Bonferroni correction for multiple-group comparisons). Likely because of the low numbers of axonal boutons in mRN as compared with pRN, the total numbers of axonal boutons found in mRN showed inconsistency across the two subgroups of intact monkeys (PM vs M1 injections; Extended Data Fig. 2-2).

The projection topography analysis revealed that both PM and M1 preferentially targeted the medial part of the pRN, without a preference along the dorsoventral axis (Fig. 2*c*, top). On the other hand, projections to mRN did not show any topographical preference (Fig. 2*c*, bottom). Quantification of the PM projection topography demonstrated a statistically significant increase of density going from lateral to medial in both the ipsilateral and contralateral pRN (Fig. 2*d*, left; p values < 0.05 , Wilcoxon signed-rank test). As far as the M1 projection topography is concerned, only ipsilateral pRN displayed preferential medial projections (Fig. 2*d*, right; p values < 0.05 , Wilcoxon signed-rank test).

Monkeys subjected to motor disorders

Given the functional importance of the RN in control of movement, we next aimed at investigating the plasticity of PM and M1 corticorubral projections following a disorder affecting motor functions. We first examined the corticorubral projection in six monkeys subjected to SCI, consisting of a cervical hemisection at C7–C8 level, (Freund et al., 2006, 2007; Beaud et al., 2008; Extended Data Fig. 3-1*a*). The BDA injections were performed unilaterally in M1 on the contralateral side. Regardless of the administration of an anti-Nogo-A antibody treatment (Extended Data Table 1-1), all six SCI monkeys exhibited a loss (or dramatic reduction) of M1 originating corticorubral projections (Fig. 3*a*; p values < 0.0071 ; residual estimation of the combined bootstrapped distributions).

Second, we sought to examine the plasticity of the corticorubral projections arising from PM or M1 in a group of monkeys ($n = 4$) experiencing PD-like symptoms (Borgognon et al., 2017, 2019). Monkeys were administered the neurotoxin MPTP to produce symptoms. After reaching a stable plateau of spontaneous functional recovery, all four monkeys received a cellular therapy treatment based on the ANCE approach (Borgognon et al., 2017, 2019). At the end of the behavioral protocol, two monkeys (LL and MY) were injected with BDA unilaterally in PM (PMd and PMv). The other two monkeys (LY and MI) were injected unilaterally in M1 (hand and arm regions; Extended Data Fig. 3-1*b*). Similar to the SCI monkeys above, both PD subgroups showed a massive reduction of corticorubral projections originating from PM and M1 (Fig. 3*b*; p values < 0.016 ; residual estimation of the combined bootstrapped distributions).

Finally, we investigated the reorganization of the corticorubral projections originating from PM in M1 cortically injured monkeys ($n = 4$), all injected with BDA unilaterally in PM, homolateral to the M1 lesion (Extended Data Fig. 3-1*c*; Extended Data Table 1-1). Regardless of the administration of an anti-Nogo-A antibody treatment (Extended Data Table 1-1), all four monkeys also expressed an extensive reduction of corticorubral projections originating from PM (Fig. 3*c*; p values < 0.01 ; residual estimation of the combined bootstrapped distributions). In summary, the corticorubral projections arising from PM or M1

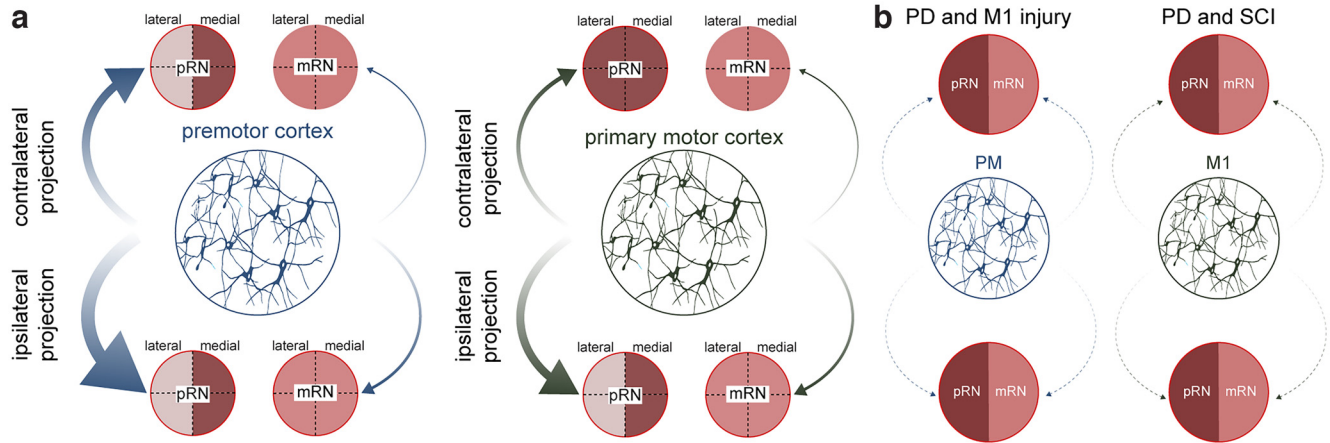


Figure 4. Schematic summary of the corticorubral projection density originating from PM or M1. *a*, PM corticorubral projection density is shown with blue arrows, whereas the M1 corticorubral projection density is shown with the green arrows. The thicker the arrow, the denser the projection. The medial preference is shown with a darker red color. *b*, The corticorubral projections after multiple motor injury/disorder is drastically reduced (dashed arrows).

were massively reduced regardless of the nature of the motor disorder tested or the respective treatment.

Discussion

Our results are largely consistent with previous studies describing the topography of the corticorubral projections originating from M1 and PM: the ipsilateral pRN is the preferential target, followed by the contralateral pRN, the ipsilateral mRN, and finally the contralateral mRN (Kuypers and Lawrence, 1967; Humphrey and Rietz, 1976; Humphrey et al., 1984; Ralston, 1994; Burman et al., 2000; Onodera and Hicks, 2009). The originality of the present study consists of the following points: (1) We reliably quantified the axonal boutons and established an extended projection topography, (2) we provided new evidence in intact monkeys that the projection from PM to pRN is denser than that from M1 to pRN (Fig. 4*a*), and (3) the corticorubral projections arising from PM and M1 were drastically reduced after motor disorders like SCI, PD, and MCI (Fig. 4*b*).

Although Burman et al. (2000) mapped the terminal boutons in the RN after injecting an anterograde tracer either in the supplementary motor area (SMA) or M1, they could not reliably compare their respective axonal bouton density. Here, we implemented a semiautomated algorithm able to tackle this problem. The algorithm detected axonal boutons within pRN and mRN and computed their respective density as well as their mediolateral and dorsoventral topography. First, PM and M1 projections preferentially targeted the medial portion of the ipsilateral pRN reflecting the somatotopical organization of the motor corticorubral projections (Larsen and Yumiya, 1980; Humphrey et al., 1984; Tokuno et al., 1995; Burman et al., 2000). Second, the projections from both PM and M1 overlapped in the medial portion of the pRN. Such convergence of motor cortical projections was also seen in the STN, where PM and SMA overlap their projections in the medial part. This convergence may reflect the internal integration of a different set of motor signals (Nambu et al., 1997). We thus propose that pRN is capable of internally segregating PM and M1 information, integrating them, and relaying the motor signal to the rubro-olivocerebellar tract. Finally, our analysis revealed that only a small proportion of the corticorubral projections reached mRN ($\sim 20\times$ less than pRN), suggesting that mRN and its rubrospinal system might work more independently from the motor cortical areas than pRN and its rubro-

olivary system. This hypothesis matches the idea that the rubrospinal system in quadrupedal animals is involved in the execution of automated movements (Orlovsky, 1972; Arshavsky et al., 1988; Kennedy, 1990). The motor cortical areas encode automated movements to a lesser extent compared with voluntary movements (Serradj et al., 2014). Therefore, one could expect that mRN may receive fewer motor commands from the cerebral cortex. Interestingly, in primate, the rubrospinal system contributes to the execution of skilled hand movements (Kuypers and Lawrence, 1967; Gibson et al., 1985; Donkelaar, 1988; Miller et al., 1993; Mewes and Cheney, 1994; Van Kan and McCurdy, 2002). Our data therefore suggest that the primate mRN may act as a primary generator of skilled hand movements autonomously from the motor cortical areas (Humphrey and Rietz, 1976). On the contrary, the motor cortical areas may contribute through pRN to sophisticated motor processing such as the acquisition and execution of conditioned reflexes (Smith, 1970; Padel et al., 1981; Ito and Oda, 1994; Pacheco-Calderon et al., 2012) and motor learning through error information encoding (Reid et al., 2009). However, most of these studies have been conducted in nonprimate animal models, where the pRN is poorly segregated in term of connectivity and morphology (Basile et al., 2021). Future experiments are needed to investigate the precise function of the corticorubral system in primates, possibly based on reversible and selective inactivation of this projection system.

Our study provides new evidence that the projection from PM to pRN is denser than that from M1 to pRN, obtained after normalizing of the number of axonal boutons in RN by the number of corticospinal axons originating from the same PM and M1 territories injected with BDA. A similar difference between PM and M1 was found for the corticosubthalamic projection (Borgognon et al., 2020), the corticotectal projection (Fregosi and Rouiller, 2017), and the corticoreticular projection (Fregosi et al., 2017). To generalize, it seems that PM is in a position to exert a stronger influence on subcortical structures than M1. We propose that this difference in projection density to subcortical structures is related to their intrinsic functions. Early electrophysiological studies demonstrated that PM is responsible for both movement preparation and execution (Wise et al., 1997; Hoshi and Tanji, 2000; Luppino and Rizzolatti, 2000), whereas M1 is more constrained to movement execution (Evarts, 1968; Thach, 1978; Georgopoulos et al., 1982, 1986; Schwartz et al., 1988; Fetz et al., 1989; Kakei et al., 1999; Dum and Strick, 2002; Mendoza and Merchant, 2014).

Indeed, earlier reports showed that PM neural activity at the population level displays increased variability across motor tasks compared with M1 (Kaufman et al., 2014). At the neural population level, PM operates in a higher-dimension fashion than M1, likely reflecting an intrinsic neural mechanism for rapid motor learning (Perich et al., 2018). PM neural signatures seem therefore to exhibit a more complex pattern of activity than M1. We proposed that these complex motor signals must be conveyed to subcortical structures that will in turn integrate them and transmit them back to the cortex via the thalamus. In that manner PM provides a neural substrate of advanced motor signals such as the transition between planning and motor execution (Inagaki et al., 2022).

The plastic changes in corticofugal projections from PM and M1 after motor injury or disorder differ depending on the lesion type, the lesion severity, and the respective tentative treatment (see above, Introduction). A lesion (or disorder) challenges the motor system requiring an adaptation to reestablish the best possible motor control. This adaptation can be achieved by remodeling projections. To the best of our knowledges, we show here for the first time a pathway that undergoes the same plastic change after multiple distinct motor injuries/disorders in primates. This uniform lesion/disorder-related adaptation of the corticorubral projection differs from other descending motor projections from PM and M1 previously observed in the same groups of monkeys (see above, Introduction). One may hypothesize that this dramatic reduction is a consequence of the disuse of the affected limb. This hypothesis is unlikely because the limb disuse was very short, lasting ~2–3 weeks, before a progressive and significant functional recovery took place during a few months, reaching a plateau of performance either spontaneously or enhanced by a treatment (Liu and Rouiller, 1999; Freund et al., 2006, 2009; Kaeser et al., 2010, 2011; Hoogewoud et al., 2013; Wyss et al., 2013). Moreover, the disuse hypothesis is not compatible with previous observations that other parallel corticofugal projections were either unchanged or even increased (see above, Introduction). Thus, this unique and uniform plasticity might be a consequence of the primitive structure of the RN, allowing the RN to play an important role after a disorder (injury) through the rubrospinal system (Rodriguez-Oroz et al., 2008) in synergy with the rubro-olivary system (Kennedy, 1990) but independent from the motor cortical areas. However, in a diffusion tensor imaging study in chronic stroke patients, the alternate motor fibers (aMF), corresponding to the nonpyramidal tract fibers, displayed high fractional anisotropy in the vicinity of the RN (Rüber et al., 2012). The authors suggested that the motor corticorubral projections play a compensatory role contributing to functional recovery. Our data are not in line with this study, which is a discrepancy that can be explained as follows. Rüber et al. (2012) could not distinguish between the corticorubral and corticoreticular tracts, as both are aMF. The recovery seen by Rüber et al. (2012) might be because of an upregulated corticoreticular projection observed in monkeys following sensorimotor cortex injury (Darling et al., 2018). Nevertheless, the primate rubrospinal neurons undergo a plastic change to facilitate their flexors and extensor muscles effects after corticospinal damage (Belhaj-Saïf and Cheney, 2000). Therefore, we suggest that the plastic changes within the RN is mediated through another mechanism than through an upregulated corticorubral projection remodeling, at least in primates. However, in rats, Ishida et al. (2016) showed a causal link between an adaptative axonal sprouting of the motor corticorubral pathway and functional recovery after stroke. This discrepancy may be the results of the striking difference between the respective motor system organization in rodents and in primates (Rouiller, 2012; Badi

et al., 2021; Sinopoulou et al., 2022). Our present observation of a dramatic reduction may represent an attempt to privilege direct access to the final output motor system at spinal cord level (via the direct corticospinal projection). The corticospinal system has been indeed proposed to play a major role in the recovery of motor symptoms after SCI (Freund et al., 2006, 2007), stroke (for review, see Jang, 2009; Pirondini et al., 2022), and PD (Underwood and Parr-Brownlie, 2021). We thus posit that reducing descending colateralization to the RN privileges direct access to the corticospinal system. This plasticity mechanism may emphasize the evolutionary difference recently reported between rodents and primates (Sinopoulou et al., 2022).

References

- Arshavsky YI, Orlovsky GN, Perret C (1988) Activity of rubrospinal neurons during locomotion and scratching in the cat. *Behav Brain Res* 28:193–199.
- Badi M, Borgognon S, O'Doherty JE, Shokur S (2021) Somatosensory Cortical stimulation for somatosensory feedback: translation from non-human primates to clinical applications. In: *Somatosensory feedback for neuroprosthetics*, Chap 13 (Güçlü B, ed), pp 413–441. Academic Press.
- Badoud S, Borgognon S, Cottet J, Chatagny P, Moret V, Fregosi M, Kaeser M, Fortis E, Schmidlin E, Bloch J, Brunet JF, Rouiller EM (2017) Effects of dorsolateral prefrontal cortex lesion on motor habit and performance assessed with manual grasping and control of force in macaque monkeys. *Brain Struct Funct* 222:1193–1206.
- Basile GA, Quartu M, Bertino S, Serra MP, Boi M, Bramanti A, Anastasi GP, Milardi D, Cacciola A (2021) Red nucleus structure and function: from anatomy to clinical neurosciences. *Brain Struct Funct* 226:69–91.
- Beaud M-L, Schmidlin E, Wannier T, Freund P, Bloch J, Mir A, Schwab ME, Rouiller EM (2008) Anti-Nogo-A antibody treatment does not prevent cell body shrinkage in the motor cortex in adult monkeys subjected to unilateral cervical cord lesion. *Bmc Neurosci* 9:5–5.
- Belhaj-Saïf A, Cheney PD (2000) Plasticity in the distribution of the red nucleus output to forearm muscles after unilateral lesions of the pyramidal tract. *J Neurophysiol* 83:3147–3153.
- Bloch J, Kaeser M, Sadeghi Y, Rouiller EM, Redmond DE, Brunet J-F (2011) Doublecortin-positive cells in the adult primate cerebral cortex and possible role in brain plasticity and development. *J Comp Neurol* 519:775–789.
- Bloch J, Brunet J-F, McEntire CRS, Redmond DE (2014) Primate adult brain cell autotransplantation produces behavioral and biological recovery in 1-methyl-4-phenyl-1,2,3,6-tetrahydropyridine-induced parkinsonian St. Kitts monkeys. *J Comp Neurol* 522:2729–2740.
- Borgognon S, Cottet J, Moret V, Chatagny P, Ginovart N, Antonescu C, Bloch J, Brunet J-F, Rouiller EM, Badoud S (2017) Enhancement of striatal dopaminergic function following autologous neural cell ecosystems (ANCE) transplantation in a non-human primate model of Parkinson's disease. *J of Alzheimer's Disease and Parkinsonism* 7:1–11.
- Borgognon S, Cottet J, Moret V, Chatagny P, Carrara L, Fregosi M, Bloch J, Brunet J-F, Rouiller EM, Badoud S (2019) Fine manual dexterity assessment after autologous neural cell ecosystem (ANCE) transplantation in a non-human primate model of Parkinson's disease. *Neurorehabil Neural Repair* 33:553–567.
- Borgognon S, Cottet J, Badoud S, Bloch J, Brunet J-F, Rouiller EM (2020) Cortical projection from the premotor or primary motor cortex to the subthalamic nucleus in intact and parkinsonian adult macaque monkeys: a pilot tracing study. *Front Neural Circuits* 14: 528993.
- Brunet J-F, Pellerin L, Arsenijevic Y, Magistretti P, Villemure J-G (2002) A novel method for *in vitro* production of human glial-like cells from neurosurgical resection tissue. *Lab Invest* 82:809–812.
- Brunet J-F, Rouiller E, Wannier T, Villemure J-G, Bloch J (2005) Primate adult brain cell autotransplantation, a new tool for brain repair? *Exp Neurol* 196:195–198.
- Brunet J-F, Redmond DE, Bloch J (2009) Primate adult brain cell autotransplantation, a pilot study in asymptomatic MPTP-treated monkeys. *Cell Transplant* 18:787–799.
- Burman K, Darian-Smith C, Darian-Smith I (2000) Macaque red nucleus: origins of spinal and olivary projections and terminations of cortical inputs. *J Comp Neurol* 423:179–196.

- Darling WG, Ge J, Morecraft KSS, Rotella DL, Pizzimenti MA, Morecraft RJ (2018) Hand motor recovery following extensive frontoparietal cortical injury is accompanied by upregulated corticoreticular projections in monkey. *J Neurosci* 38:6323–6339.
- Dum R, Strick P (2002) Motor areas in the frontal lobe of the primate. *Physiol Behav* 77:677–682.
- Evarts EV (1968) Relation of pyramidal tract activity to force exerted during voluntary movement. *J Neurophysiol* 31:14–27.
- Fetz EE, Cheney PD, Mewes K, Palmer S (1989) Control of forelimb muscle activity by populations of corticomotoneuronal and rubromotoneuronal cells. *Prog Brain Res* 80:437–449.
- Fregosi M, Rouiller EM (2017) Ipsilateral corticotectal projections from the primary, premotor and supplementary motor cortical areas in adult macaque monkeys: a quantitative anterograde tracing study. *Eur J Neurosci* 46:2406–2415.
- Fregosi M, Contestabile A, Hamadjida A, Rouiller EM (2017) Corticobulbar projections from distinct motor cortical areas to the reticular formation in macaque monkeys. *Eur J Neurosci* 45:1379–1395.
- Fregosi M, Contestabile A, Badoud S, Borgognon S, Cottet J, Brunet J-F, Bloch J, Schwab ME, Rouiller EM (2018) Changes of motor corticobulbar projections following different lesion types affecting the central nervous system in adult macaque monkeys. *Eur J Neurosci* 48:2050–2070.
- Fregosi M, Contestabile A, Badoud S, Borgognon S, Cottet J, Brunet J-F, Bloch J, Schwab ME, Rouiller EM (2019) Corticotectal projections from the premotor or primary motor cortex after cortical lesion or parkinsonian symptoms in adult macaque monkeys: a pilot tracing study. *Front Neuroanat* 13:1193.
- Freund P, Schmidlin E, Wannier T, Bloch J, Mir A, Schwab ME, Rouiller EM (2006) Nogo-A-specific antibody treatment enhances sprouting and functional recovery after cervical lesion in adult primates. *Nat Med* 12:790–792.
- Freund P, Wannier T, Schmidlin E, Bloch J, Mir A, Schwab ME, Rouiller EM (2007) Anti-Nogo-A antibody treatment enhances sprouting of corticospinal axons rostral to a unilateral cervical spinal cord lesion in adult macaque monkey. *J Comp Neurol* 502:644–659.
- Freund P, Schmidlin E, Wannier T, Bloch J, Mir A, Schwab ME, Rouiller EM (2009) Anti-Nogo-A antibody treatment promotes recovery of manual dexterity after unilateral cervical lesion in adult primates—re-examination and extension of behavioral data. *Eur J Neurosci* 29:983–996.
- Georgopoulos AP, Kalaska JF, Caminit R, Massey JT (1982) On the relations between the direction of two-dimensional arm movements and cell discharge in primate motor cortex. *J Neurosci* 2:1527–1537.
- Georgopoulos AP, Schwartz AB, Kettner RE (1986) Neuronal population coding of movement direction. *Science* 233:1416–1419.
- Gibson AR, Houk JC, Kohlerman NJ (1985) Relation between red nucleus discharge and movement parameters in trained macaque monkeys. *J Physiol* 358:551–570.
- Gruber P, Gould DJ (2010) The red nucleus: past, present, and future. *Neuroanatomy* 9:1–3.
- Guan X, Xuan M, Gu Q, Huang P, Liu C, Wang N, Xu X, Luo W, Zhang M (2017) Regionally progressive accumulation of iron in Parkinson's disease as measured by quantitative susceptibility mapping. *Nmr Biomed* 30:e3489.
- Hamadjida A, Wyss AF, Mir A, Schwab ME, Belhaj-Saif A, Rouiller EM (2012) Influence of anti-Nogo-A antibody treatment on the reorganization of callosal connectivity of the premotor cortical areas following unilateral lesion of primary motor cortex (M1) in adult macaque monkeys. *Exp Brain Res* 223:321–340.
- Hoogewoud F, Hamadjida A, Wyss AF, Mir A, Schwab ME, Belhaj-Saif A, Rouiller EM (2013) Comparison of functional recovery of manual dexterity after unilateral spinal cord lesion or motor cortex lesion in adult macaque monkeys. *Front Neurol* 4:101.
- Hoshi E, Tanji J (2000) Integration of target and body-part information in the premotor cortex when planning action. *Nature* 408:466–470.
- Humphrey DR, Rietz RR (1976) Cells of origin of corticorubral projections from the arm area of primate motor cortex and their synaptic actions in the red nucleus. *Brain Res* 110:162–169.
- Humphrey DR, Gold R, Reed DJ (1984) Sizes, laminar and topographic origins of cortical projections to the major divisions of the red nucleus in the monkey. *J Comp Neurol* 225:75–94.
- Inagaki HK, Chen S, Ridder MC, Sah P, Li N, Yang Z, Hasanbegovic H, Gao Z, Gerfen CR, Svoboda K (2022) A midbrain-thalamus-cortex circuit reorganizes cortical dynamics to initiate movement. *Cell* 185:1065–1081.e23.
- Ishida A, Isa K, Umeda T, Kobayashi K, Kobayashi K, Hida H, Isa T (2016) Causal link between the cortico-rubral pathway and functional recovery through forced impaired limb use in rats with stroke. *J Neurosci* 36:455–467.
- Ito M, Oda Y (1994) Electrophysiological evidence for formation of new corticorubral synapses associated with classical conditioning in the cat. *Exp Brain Res* 99:277–288.
- Jang SH (2009) The role of the corticospinal tract in motor recovery in patients with a stroke: A review. *Neurorehabilitation* 24:285–290.
- Kaesler M, Wyss AF, Bashir S, Hamadjida A, Liu Y, Bloch J, Brunet J-F, Belhaj-Saif A, Rouiller EM (2010) Effects of unilateral motor cortex lesion on ipsilesional hand's reach and grasp performance in monkeys: relationship with recovery in the contralesional hand. *J Neurophysiol* 103:1630–1645.
- Kaesler M, Brunet J-F, Wyss A, Belhaj-Saif A, Liu Y, Hamadjida A, Rouiller EM, Bloch J (2011) Autologous adult cortical cell transplantation enhances functional recovery following unilateral lesion of motor cortex in primates: a pilot study. *Neurosurgery* 68:1405–1407.
- Kakei S, Hoffman DS, Strick PL (1999) Muscle and movement representations in the primary motor cortex. *Science* 285:2136–2139.
- Kaufman MT, Churchland MM, Ryu SI, Shenoy KV (2014) Cortical activity in the null space: permitting preparation without movement. *Nat Neurosci* 17:440–448.
- Kennedy PR (1990) Corticospinal, rubrospinal and rubro-olivary projections: a unifying hypothesis. *Trends Neurosci* 13:474–479.
- Kuypers HG, Lawrence DG (1967) Cortical projections to the red nucleus and the brain stem in the rhesus monkey. *Brain Res* 4:151–188.
- Larsen KD, Yumiya H (1980) The red nucleus of the monkey. *Exp Brain Res* 40:393–404.
- Lemon RN (2008) Descending pathways in motor control. *Annu Rev Neurosci* 31:195–218.
- Liu Y, Rouiller EM (1999) Mechanisms of recovery of dexterity following unilateral lesion of the sensorimotor cortex in adult monkeys. *Exp Brain Res* 128:149–159.
- Luppino G, Rizzolatti G (2000) The organization of the frontal motor cortex. *News Physiol Sci* 15:219–224.
- Massion J (1988) Red nucleus: past and future. *Behav Brain Res* 28:1–8.
- Mendoza G, Merchant H (2014) Motor system evolution and the emergence of high cognitive functions. *Prog Neurobiol* 122:73–93.
- Mewes K, Cheney PD (1994) Primate rubromotoneuronal cells: parametric relations and contribution to wrist movement. *J Neurophysiol* 72:14–30.
- Miller LE, van Kan PL, Sinkjaer T, Andersen T, Harris GD, Houk JC (1993) Correlation of primate red nucleus discharge with muscle activity during free-form arm movements. *J Physiol* 469:213–243.
- Nambu A, Tokuno H, Inase M, Takada M (1997) Corticosubthalamic input zones from forelimb representations of the dorsal and ventral divisions of the premotor cortex in the macaque monkey: comparison with the input zones from the primary motor cortex and the supplementary motor area. *Neurosci Lett* 239:13–16.
- Onodera S, Hicks TP (2009) A comparative neuroanatomical study of the red nucleus of the cat, macaque and human. *Plos One* 4:e6623.
- Orlovsky GN (1972) The effect of different descending systems on flexor and extensor activity during locomotion. *Brain Res* 40:359–371.
- Pacheco-Calderon R, Carretero-Guillen A, Delgado-Garcia JM, Gruart A (2012) Red nucleus neurons actively contribute to the acquisition of classically conditioned eyelid responses in rabbits. *J Neurosci* 32:12129–12143.
- Padel Y, Angaut P, Massion J, Sedan R (1981) Comparative study of the posterior red nucleus in baboons and gibbons. *J Comp Neurol* 202:421–438.
- Paxinos G, Huang XF, Toga AW (2000) The rhesus monkey brain in stereotaxic coordinates. Amsterdam: Elsevier.
- Perich MG, Gallego JA, Miller LE (2018) A neural population mechanism for rapid learning. *Neuron* 100:964–976.e7.
- Philippens I, Wubben JA, Franke SK, Hofman S, Langermans JAM (2019) Involvement of the red nucleus in the compensation of parkinsonism may explain why primates can develop stable Parkinson's disease. *Sci Rep* 9:880.
- Pirondini E, Carranza E, Balaguer J-M, Sorensen E, Weber DJ, Krakauer JW, Capogrosso M (2022) Poststroke arm and hand paresis: should we target the cervical spinal cord? *Trends Neurosci* 45:568–578.

- Ralston DD (1994) Corticorubral synaptic organization in *Macaca fascicularis*: A study utilizing degeneration, anterograde transport of WGA-HRP, and combined immuno-GABA-gold technique and computer-assisted reconstruction. *J Comp Neurol* 350:657–673.
- Reid EK, Norris SA, Taylor JA, Hathaway EN, Smith AJ, Yttri EA, Thach WT (2009) Is the parvocellular red nucleus involved in cerebellar motor learning? *Curr Trends Neurology* 3:15–22.
- Rodriguez-Oroz MC, Rodriguez M, Leiva C, Rodriguez-Palmero M, Nieto J, Garcia-Garcia D, Zubieta JL, Cardiel C, Obeso JA (2008) Neuronal activity of the red nucleus in Parkinson's disease. *Mov Disord* 23:908–911.
- Rouiller EM (2012) What can we learn from animal models? In: *Routledge Handbook of Motor Control and Motor Learning* (Gollhofer A, Taube W, Nielsen JB, eds), pp 29–49. London: Routledge.
- Rouiller EM, Tanne J, Moret V, Kermadi I, Boussaoud D, Welker E (1998) Dual morphology and topography of the corticothalamic terminals originating from the primary, supplementary motor, and dorsal premotor cortical areas in macaque monkeys. *J Comp Neurol* 396:169–185.
- Rouiller EM, Babalian A, Kazennikov O, Moret V, Yu X-H, Wiesendanger M (1994) Transcallosal connections of the distal forelimb representations of the primary and supplementary motor cortical areas in macaque monkeys. *Exp Brain Res* 102:227–243.
- Rüber T, Schlaug G, Lindenberg R (2012) Compensatory role of the corticorubro-spinal tract in motor recovery after stroke. *Neurology* 79:515–522.
- Schwartz AB, Kettner RE, Georgopoulos AP (1988) Primate motor cortex and free arm movements to visual targets in three-dimensional space. I. Relations between single cell discharge and direction of movement. *J Neurosci* 8:2913–2927.
- Serradj N, Paixão S, Sobocki T, Feinberg M, Klein R, Kullander K, Martin JH (2014) EphA4-mediated ipsilateral corticospinal tract misprojections are necessary for bilateral voluntary movements but not bilateral stereotypic locomotion. *J Neurosci* 34:5211–5221.
- Sinopoulou E, Rosenzweig ES, Conner JM, Gibbs D, Weinholtz CA, Weber JL, Brock JH, Nout-Lomas YS, Ovruchsky E, Takashima Y, Biane JS, Kumamaru H, Havton LA, Beattie MS, Bresnahan JC, Tuszynski MH (2022) Rhesus macaque versus rat divergence in the corticospinal projectome. *Neuron* 110:2970–2983.e4.
- Smith AM (1970) The effects of rubral lesions and stimulation on conditioned forelimb flexion responses in the cat. *Physiol Behav* 5:1121–1126.
- ten Donkelaar HJ (1988) Evolution of the red nucleus and rubrospinal tract. *Behav Brain Res* 28:9–20.
- Thach WT (1978) Correlation of neural discharge with pattern and force of muscular activity, joint position, and direction of intended next movement in motor cortex and cerebellum. *J Neurophysiol* 41:654–676.
- Tokuno H, Takada M, Nambu A, Inase M (1995) Somatotopical projections from the supplementary motor area to the red nucleus in the macaque monkey. *Exp Brain Res* 106:351–355.
- Underwood CF, Parr-Brownlie LC (2021) Primary motor cortex in Parkinson's disease: functional changes and opportunities for neurostimulation. *Neurobiol Dis* 147:105159.
- Van Kan PLE, McCurdy ML (2002) Contribution of primate magnocellular red nucleus to timing of hand reshaping during reaching to grasp. *J Neurophysiol* 87:1473–1487.
- Wang J-Y, Zhuang Q-Q, Zhu L-B, Zhu H, Li T, Li R, Chen S-F, Huang C-P, Zhang X, Zhu J-H (2016) Meta-analysis of brain iron levels of Parkinson's disease patients determined by postmortem and MRI measurements. *Sci Rep* 6:36669.
- Wise SP, Boussaoud D, Johnson PB, Caminiti R (1997) Premotor and parietal cortex: corticocortical connectivity and combinatorial computations. *Annu Rev Neurosci* 20:25–42.
- Wyss AF, Hamadjida A, Savidan J, Liu Y, Bashir S, Mir A, Schwab ME, Rouiller EM, Belhaj-Saif A (2013) Long-term motor cortical map changes following unilateral lesion of the hand representation in the motor cortex in macaque monkeys showing functional recovery of hand functions. *Restor Neurol Neurosci* 31:733–760.
- Yeo SS, Jang SH (2010) Changes in red nucleus after pyramidal tract injury in patients with cerebral infarct. *Neurorehabilitation* 27:373–377.